# Nanoscale

Check for updates

# Electronic structure of cobalt valence tautomeric molecules in different environments†

Esha Mishra, [a] Thilini K. Ekanayaka, [a] Theodoros Panagiotakopoulos, [b]
Duy Le, [b] Talat S. Rahman, *[b] Ping Wang, [c] Kayleigh A. McElveen,[d]
Jared P. Phillips, [e] M. Zaid Zaz,[a] Saeed Yazdani, [e] Alpha T. N'Diaye, [f]
Rebecca Y. Lai, [d] Robert Streubel, *[a,g] Ruihua Cheng,[e] Michael Shatruk [c] and
Peter A. Dowben *[a]

*aDepartment of Physics and Astronomy, University of Nebraska-Lincoln, Lincoln,
NE 68588, USA. E-mail: Streubel@unl.edu, pdowben@unl.edu*
*bDepartment of Physics, University of Central Florida, Orlando, FL 32816, USA.
E-mail: talat@ucf.edu*
*cDepartment of Chemistry and Biochemistry, Florida State University, Tallahassee,
FL 32306, USA*
*dDepartment of Chemistry, University of Nebraska-Lincoln, Lincoln, NE, 68588, USA*
*eDepartment of Physics, Indiana University-Purdue University Indianapolis,
Indianapolis, Indiana 46202, USA*
*fAdvanced Light Source, Lawrence Berkeley National Laboratory, Berkeley, CA 94720,
USA*
*gNebraska Center for Materials and Nanoscience, University of Nebraska-Lincoln,
Lincoln, NE 68588, USA*

Future molecular microelectronics require the electronic conductivity of the device to be tunable without impairing the voltage control of the molecular electronic properties. This work reports the influence of an interface between a semiconducting polyaniline polymer or a polar poly-D-lysine molecular film and one of two valence tautomeric complexes, i.e., $[Co^{III}(SQ)(Cat)(4\text{-}CN\text{-}py)_2]$ $\leftrightarrow$ $[Co^{II}(SQ)_2(4\text{-}CN\text{-}py)_2]$ and $[Co^{III}(SQ)(Cat)(3\text{-}tpp)_2]$ $\leftrightarrow$ $[Co^{II}(SQ)_2(3\text{-}tpp)_2]$. The electronic transitions and orbitals are identified using X-ray photoemission, X-ray absorption, inverse photoemission, and optical absorption spectroscopy measurements that are guided by density functional theory. Except for slightly modified binding energies and shifted orbital levels, the choice of the underlying substrate layer has little effect on the electronic structure. A prominent unoccupied ligand-to-metal charge transfer state exists in $[Co^{III}(SQ)(Cat)(3\text{-}tpp)_2]$ $\leftrightarrow$ $[Co^{II}(SQ)_2(3\text{-}tpp)_2]$ that is virtually insensitive to the interface between the polymer and tautomeric complexes in the $Co^{II}$ high-spin state.

## 1 Introduction

Spin-crossover (SCO)[1] and valence tautomerism, an intra-molecular redox-isomerism,[2–5] provide versatile and reversible means to change the spin state of local-moment molecules. Transitioning between the low-spin (LS) and high-spin (HS) electronic configurations profoundly affects the structural, magnetic, optical, and resistive properties.[6–23] Isothermal voltage-controlled switching of the spin state has been demonstrated in Fe(II) SCO complexes,[24–26] opening a route to higher energy efficiency of non-volatile memory[26] and other types of electronic and sensing devices.[24–28] The conductivity of Fe(II)-based SCO systems can be further enhanced by adding organic semiconducting polymers, such as polyaniline (PANI) and polar poly-D-lysine (PDL),[28,29] and select molecules.[30–37] Even interfaces can improve conductivity and mobility within adjacent SCO layers and it is likely that this also holds for valence tautomeric films.

Entropy calculations suggest that the transition between LS and HS states is more facile in Co(II) than in Fe(II) complexes,[38] ultimately requiring smaller voltages to operate molecular

*Robert Streubel leverages local inversion symmetry breaking in solid-state materials to tailor magnetic and magneto-transport properties in nanostructures, amorphous materials, and molecular magnets. Robert graduated in 2011 from the TU Dresden, Germany with a Physics Diplom (M.S.) and received his doctoral degree (Dr. rer. nat.) in Physics in 2015 from TU Chemnitz, Germany for his work carried out at the Leibniz Institute for Solid State and Materials Research Dresden, Germany. Before joining the University of Nebraska-Lincoln in 2020 as an Assistant Professor in the Department of Physics and Astronomy, he worked as a post-doctoral researcher at Berkeley Lab's Materials Sciences Division.*

**Robert Streubel**

devices. Co-based complexes are also more stable in an aqueous environment than their iron counterpart as is evident from extensive electrochemical studies.[11,39–45] The electrochemical switching requires very modest voltages[11,39–45] and the few fabricated devices hint at even smaller voltages for conductivity and spin-state switching.[40] Voltage-controlled switching should extend to electric field switching of Co-based complexes exhibiting valence tautomerism[46] which are regarded as prospective organic microelectronics devices.[2,5,19]

Many of the existing valence tautomers are Co complexes[2–7,9,11–17,19,21,47–71] in which the ligand–metal interaction is key to valence tautomerism, optically driven spin state transitions, and photo-induced valence tautomerism. The existence of an intermediate ligand-to-metal charge transfer (LMCT) state[3,14–16] that is unoccupied in the ground state is critical due to optical selection rules and forbidden spin–flip transitions. Hence, the optical switching dynamics are complicated, involving a direct transition from the LS Co(III) d$^6$ electronic configuration ground state to a photo-induced excited LMCT state. The latter decays to a HS state through several out-of-equilibrium physio-chemical processes,[3,15,16,63] making the identification of the LMCT state challenging.[3,14–16,21] Assigning the LMCT state to an unoccupied molecular orbital helps in identifying this transient excited state.

Here, we report the electronic structure and orbital levels of two cobalt-based valence tautomeric systems and their dependence on the local environment that varies with the choice of substrate layers and is essential for any optical, optoelectronic, and microelectronics application. Our study concerns the LS and HS state combination of $[Co^{III}(SQ)(Cat)(4\text{-}CN\text{-}py)_2] \leftrightarrow [Co^{II}(SQ)_2(4\text{-}CN\text{-}py)_2]$ (Cat = 3,5-di-*tert*-butylcatecholate, SQ = 3,5-di-*tert*-butylsemiquinonate, 4-CN-py = 4-cyanopyridine) and of $[Co^{III}(SQ)(Cat)(3\text{-}tpp)_2] \leftrightarrow [Co^{II}(SQ)_2(3\text{-}tpp)_2]$ (3-tpp = 3-thienylpyridine) with and without the addition of an adjacent semiconducting polymer PANI and PDL layer. Throughout the manuscript, Co-py and Co-tpp will be used to refer to the first and second tautomeric complex, respectively. The chemical structures of Co-py and Co-tpp are virtually the same except for two modified end groups that have a profound impact on the orbital levels and hybridization of the local-moment ion. The experiments, leveraging X-ray absorption, X-ray photoemission, optical absorption, and inverse photoemission spectroscopies, are guided by *ab initio* calculations to identify relevant electronic transitions and orbitals. Aside from slightly modified binding energies and shifted orbital levels, the electronic structure and identified the LMCT state remain unperturbed, independent of the interface between HS Co-py and PANI or PDL and Co-tpp and PANI or PDL.

## 2 Experimental

### 2.1 Synthesis

Co-py was synthesized as previously reported.[72] This complex is in the HS state at room temperature as the valence tautomerism-SCO transition occurs at ≈110 K. Both crystal structure and purity were confirmed by correlating the room-temperature powder X-ray diffraction data obtained with a Panalytical XPert Pro X-ray diffractometer equipped with an XCelerator detector and a Cu-K$_\alpha$ source with the modeled data (CrystalDiffract software; ESI Fig. 1†). For the synthesis of Co-tpp, a solution of $[Co(SQ)_2]_4$ (270 mg, 0.13 mmol) in 8 mL of toluene is layered on top of a solution of 3-tpp (172 mg, 1.07 mmol) in 5 mL of dichloromethane. Dark-blue crystals that form after two weeks were harvested, washed with toluene, and dried under vacuum at 100 °C for 24 hours to yield the desired product as dark-green powder (180 mg, or 42%). The elemental analysis for C$_{46}$H$_{55}$CoN$_2$O$_4$S$_2$ (Co-tpp) reveals: found (calculated) C 66.84 (67.13), H 6.73 (6.74), N 3.31 (3.40). The crystal structure determination was carried out by single-crystal X-ray diffraction on a Rigaku Synergy-S diffractometer using a Mo-K$_\alpha$ radiation source. The final structure of Co-tpp has been deposited with the Cambridge Crystallographic Data Centre (reference 2221051). Magnetic properties of Co-tpp are analyzed in terms of the magnetic susceptibility $\chi$ recorded with a Magnetic Property Measurement System (MPMS-XL, Quantum Design), yielding a valence tautomerism-SCO transition temperature of ≈370 K (ESI Fig. 2†). The conversion is incomplete even at 400 K where the $\chi T$ value reaches ≈3.1 emu K mol$^{-1}$ remaining shy of ≈3.7 emu K mol$^{-1}$ of the HS Co-py state.[65] Assuming similar $\chi T$ values for HS Co-py and HS Co-tpp due to similar coordination environment and electronic structure, we estimate that roughly 80% of the Co-tpp molecules are in the HS state at 400 K. The low-temperature state reveals a $\chi T$ value of ≈0.6 emu K mol$^{-1}$, which is close to the spin-only expectation value (≈0.38 emu K mol$^{-1}$) for $S = 1/2$ LS state. The discrepancy between experimental and analytical data is likely caused by a sizable fraction of molecules trapped in the HS state at low temperature.

Polyaniline was synthesized using an oxidative polymerization method, where 10 mL of a 1 M hydrochloric acid (HCl) solution of 0.25 M ammonium persulfate (APS) is added to 30 mL of a 0.25 M solution of aniline in water. The suspension was stirred for 6 hours at 0 °C and overnight at room temperature. The resulting green precipitate was washed with 1 M HCl, ethanol, and water until the supernatant turned clear and left to dry in vacuum. Mixing 5 mg of PDL hydrobromide (Sigma Aldrich) and PANI in 6.25 mL and 4 mL of distilled water yields poly-D-lysine (PDL) and polyaniline (PANI), respectively. Solutions of HS Co-py and Co-tpp were prepared by mixing 5 mg of the corresponding complex in 4 mL of toluene. 150 μL of the Co-py or Co-tpp solutions are drop-casted either directly on a $(1 \times 1)$ cm$^2$ HOPG substrate or on top of dried PDL or PANI substrate layers on HOPG. The dried polymer films were prepared using 150 μL of either PDL or PANI solution. The HOPG substrate was chosen as it is one of the few substrates that reliably does not perturb the SCO molecular spin state nor the spin state transition.[73]

### 2.2 Experiment

X-ray absorption spectroscopy (XAS) was carried out at 300 K in the total electron yield mode at the Advanced Light Source

(bending magnet beamline 6.3.1). X-ray photoemission spectroscopy (XPS) was performed at different temperatures using an Al $K_\alpha$ X-ray source with a photon energy of 1486.6 eV. Inverse photoemission spectroscopy (IPES) was conducted using an electron gun and power supply system (ELG-2/EGPS-1022) from Kimball Physics, Inc. combined with a channeltron detector. Optical absorption spectroscopy was performed using a Thermo Fisher Scientific G10S UV-Vis. The XPS spectra are analyzed using CasaXPS and Shirley background. The number of peaks is chosen to guarantee best fit. The binding energies are referenced to the carbon 1s peak at 284.7 eV to compensate for charging effects. Owing to negligible contributions from inelastic scattering of excited electrons, the commonly used product functions consisting of an asymmetric Lorentzian and Gaussian[74,75] to fit XAS and IPES spectra can be simplified to a finite set of symmetric Gaussians. The corresponding resonances are assigned to groups of orbital levels derived from density functional theory.

### 2.3 Theory

The structural and chemical complexity of valence tautomeric systems requires the numerical modeling of the partial density of states to identify contributions of ligands and the Co metal center to the absorption spectra. Density functional theory (DFT) with the projector-augmented wave (PAW)[76,77] and the plane-wave basis set, as implemented in the Vienna *ab initio* Simulation Package (VASP),[78] was used to calculate the electronic structures of the unoccupied states of single-molecule Co-py and Co-tpp in the HS state. We employed the hybrid functional Heyd–Scuseria–Ernzerhof (HSE06)[79,80] to calculate the electronic structure of the molecules as it has proven to be a reliable predictor for molecular systems, including the valence and conduction bandwidth and HOMO–LUMO gap.[81,82] This approach is computationally demanding. Prior to determining the electronic structure, we have thus obtained the molecular geometric structure through ionic relaxation using the generalized-gradient approximation (GGA) in the form of the Perdew–Burke–Ernzerhof (PBE)[83,84] functional together with DFT-D3 correction[85] to describe the electronic exchange correlation. The strong self-interaction of the Co 3d electrons during the structure relaxation is modeled by a Hubbard-like repulsion term ($U = 3.0$ eV) following the method by Dudarev *et al.*[86] The electron kinetic energy cut-off for plane-wave expansion is 500 eV. The simulation supercell includes one molecule surrounded by a 1.5 nm-thick vacuum shell. The Brillouin zone was sampled with one point at the zone center. Gaussian smearing was used for the integration over the Brillouin zone with a standard deviation $\sigma = 0.1$ eV during relaxation and $\sigma = 0.05$ eV for electronic structure calculation. Convergence for electronic cycles and ionic relaxation was reached at $10^{-6}$ eV and $10^{-2}$ eV Å$^{-1}$, respectively. Our discussion focuses on the HS Co-py and Co-tpp complexes since calculations of the electronic structure in the LS state are less accurate due to an underestimated correlation energy yielding a smaller energy gap (lower LUMO levels) than for the HS state and experimentally observed (ESI Fig. 3†). For both LS Co-py

and Co-tpp complexes, the cobalt orbitals are hybridized with ligand orbitals in contrast to the HS state discussed below.

## 3 Results and discussion

### 3.1 Partial density of unoccupied states

The partial density of states derived from DFT reveals a strong spin-polarized SQ ligand contribution near the Fermi level (0 eV) and 1.5 to 2 eV above (Fig. 1). The unoccupied ligand orbitals of 4-CN-py and 3-tpp for HS Co-py and HS Co-tpp, respectively, appear at 2.5 to 4 eV. The 3-tpp orbitals are shifted by +0.5 eV with respect to the 4-CN-py levels. Moreover, the Co-py complex has two 4-CN-py levels compared to three 3-tpp orbitals in the depicted energy range. Aside from the third 3-tpp orbital located at 3.8 eV that is heavily hybridized with cobalt orbitals, the low-lying unoccupied molecular orbitals are non-polarized and reveal a minor cobalt contribution indicating weak orbital hybridization. The latter is also evident from the electron orbitals themselves, displayed as iso-energy surfaces in Fig. 1. As a result, the orbital of the unoccupied cobalt level in Co-py lying at 3.7 eV is localized in contrast to the two cobalt levels in Co-tpp that are symmetric around the third 3-tpp orbital level at 3.7 and 3.9 eV (Fig. 1). Considering the small differences in the chemical structure and similar coordination environment of both tautomeric molecules, it is remarkable that the spin-polarized cobalt orbitals span the entire Co-tpp molecular plane likely yielding a large magnetoresistance.

To correlate the modeled orbital levels with spectroscopy studies, orbitals with similar energies are grouped and labeled using roman numerals (Fig. 1). The unoccupied electronic states were experimentally probed by means of soft X-ray (XAS) and optical absorption as well as inverse photoemission (IPES) spectroscopies. The varying information depth of IPES ($\approx 2$ nm) and XAS using total electron yield ($\approx 6$ nm) allows to distinguish ligand and metal contributions. Additionally, the selection rules for IPES and XAS are distinct.[87] XAS probes dipole transitions (p $\rightarrow$ d) where the symmetry of the system plays a minor role. The selection of symmetry groups in IPES is much more narrow providing insight into the net molecule orientation. Based on the orbital distribution (Fig. 1), we expect a weak IPES signal for the central Co atom in Co-py and a strong IPES signal for SQ levels. The signal intensity is to be seen in reference to the corresponding XAS signal. To compare XAS with IPES spectra, it is critical to account for the core level binding energy offset, accessible through X-ray photoemission spectroscopy (XPS). By these means, the photon energies used in XAS can be correlated with the unoccupied state binding energies relative to the Fermi energy $E_F$ as $E - E_F$. In cationic materials, the chemical potential (Fermi energy) aligns close to the highest occupied molecular orbital (HOMO) and the gap between the HOMO and the lowest unoccupied molecular orbital (LUMO) is merely the binding energy in IPES. The same approach was used to represent the partial density of unoccupied states (Fig. 1) and allows to probe the unoccupied density of states leveraging XAS, IPES, and optical absorption.
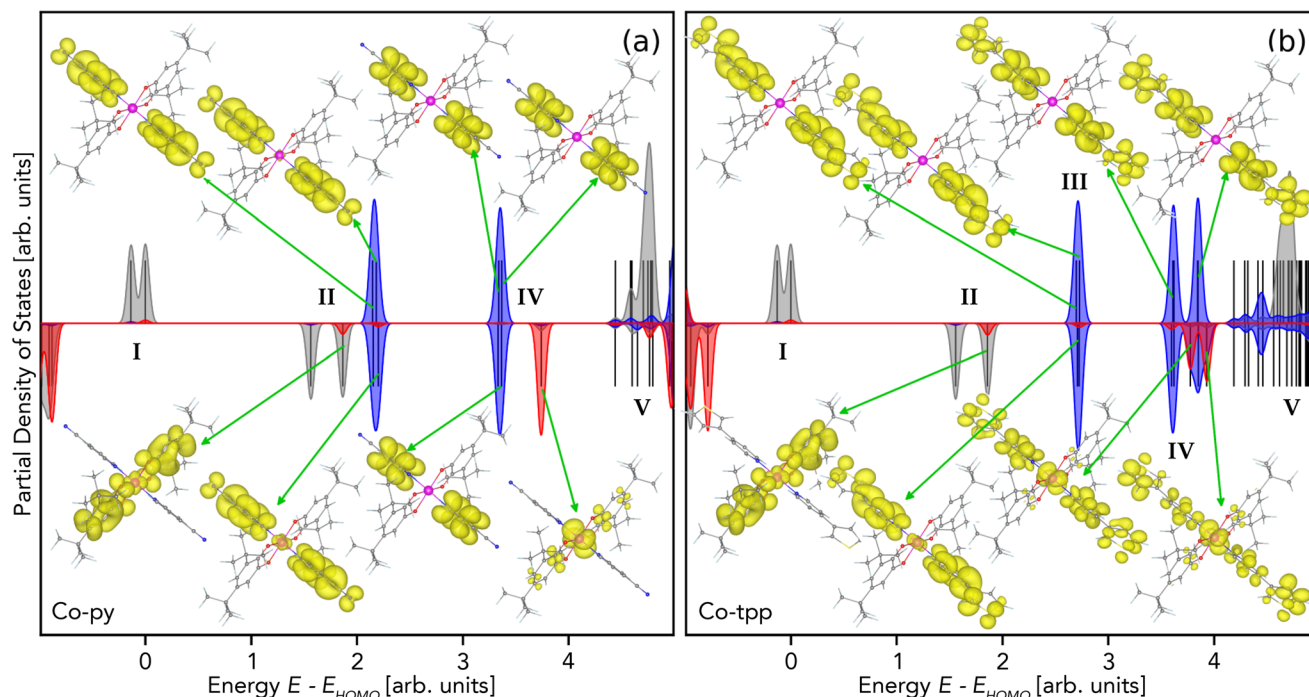
**Fig. 1** Partial density of states derived from *ab initio* Heyd–Scuseria–Ernzerhof calculations. Contributions of cobalt (red), SQ ligand (gray), and 4-CN-py or 3-tpp ligand (blue) to the largely unoccupied electronic structure of (a) high-spin state Co-py and (b) high-spin state Co-tpp. Spin-up and spin-down components are displayed in the upper and lower half of each panel, respectively. The wave function of select unoccupied molecular orbitals are depicted as insets with an iso-surface value of 0.005 e⁻ Å⁻³. The zero-energy level is set to the highest occupied molecular orbital (HOMO) level. Orbitals with similar energies are grouped and labeled using roman numerals for correlation with spectroscopy studies. Group III is absent in Co-py.

## 3.2 Influence of adjacent substrate layer

XPS near the Co $2p_{3/2}$ absorption edge of HS Co-py and Co-tpp molecular films reveals minor changes in the fine structure for films with and without adjacent PANI or PDL layers, including, in particular, the Co $2p_{3/2}$ multiplet structure around 781 eV (Fig. 2, Table 1). These values coincide with binding energies reported for other Co $2p_{3/2}$ valence tautomeric complexes[21] and show no evidence of a high-binding energy features indicative of oxidation.[21,88] All spectra are taken above the SCO transition temperature, which is 110 K for Co-py[72] and 370 K for Co-tpp (ESI Fig. 1†). The broad valence tautomerism-SCO transition infers that at least 60% of the Co-tpp molecules are in the HS state at 380 K. This estimate is expected to be well below the actual HS state population which typically increases under X-ray irradiation.[72] The XPS Co $2p_{3/2}$ spectra contain, due to its highly out-of-equilibrium nature of excitation, satellites of multiplets, two-hole bound states (shake-ups), or shake-offs. Satellite features at 4 and 6 eV larger binding energy than the principal Co $2p_{3/2}$ core level energy are consistent with excitations from the HOMO to the LMCT state discussed below. Note that multiplets resulting from configuration interactions and *j*–*J* coupling in the photoemission final state cannot be excluded. Overall, the resonances of Co-tpp are shifted toward smaller (larger) binding energies on PDL (PANI) substrate layers with respect to HOPG indicating an anionic (cationic) character (Fig. 2, Table 1). HS Co-py becomes more
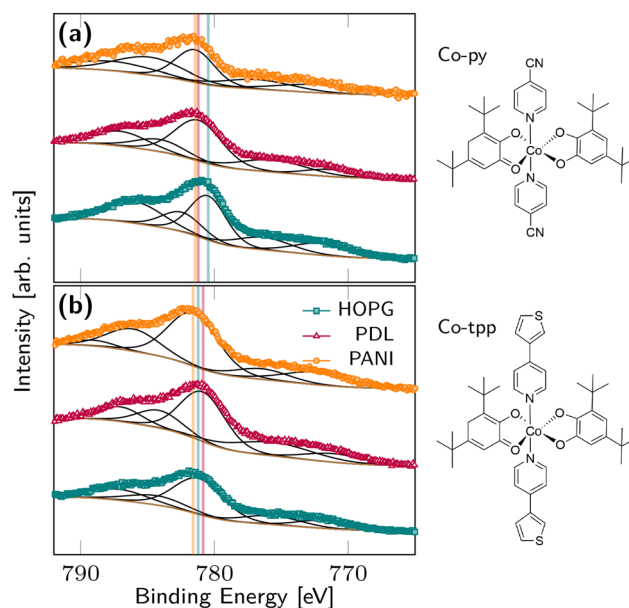


**Fig. 2** X-ray photoemission spectra of (a) HS Co-py and (b) Co-tpp on different organic substrate layers near the cobalt $2p_{3/2}$ absorption edges recorded at 320 K and 380 K, respectively. Vertical lines indicate the Co $2p_{3/2}$ core level energy. The spectra are fitted using five resonances after removing the Shirley background (brown curve) and vertically shifted for visibility. The total fitting curve is plotted behind the experimental data.

**Table 1** Resonance energies of core level excitations derived from X-ray photoemission spectra plotted in Fig. 2. (C) and (A) refer to cationic and anionic character or larger and smaller binding energies with respect to HOPG, respectively

| Substrate | $E_1$ [eV] | $E_2$ [eV] | $E_3$ [eV] | $E_4$ [eV] | $E_5$ [eV] |
|---|---|---|---|---|---|
| **Co-py** | | | | | |
| HOPG | 771.9 | 776.4 | 780.5 | 782.5 | 786.0 |
| PDL (C) | 771.4 | 775.6 | 781.2 | 784.1 | 787.0 |
| PANI (C) | 772.2 | 776.8 | 781.4 | 784.8 | 787.6 |
| **Co-tpp** | | | | | |
| HOPG | 771.8 | 775.7 | 781.2 | 784.3 | 787.1 |
| PDL (A) | 771.1 | 775.6 | 780.8 | 784.1 | 787.0 |
| PANI (C) | 772.3 | 776.4 | 781.6 | 786.1 | 789.0 |

cationic in contact with either PDL or PANI films (Fig. 2, Table 1). This tendency has ramifications for molecular transistors.

XAS tends to show the spectral weight of unoccupied states associated with the initial-state core level yielding a less complex spectra than XPS. The Co 2p XAS spectra taken at 300 K for a HS Co-py molecular film on HOPG, PDL, and PANI substrate layers are nearly the same as are the spectra for Co-tpp on HOPG, PDL, and PANI substrate layers (Fig. 3) and resemble those previously reported.[47,54,70,71] Notably, the spectra differ from XAS studies of cobalt-based SCO complexes in the LS state that do not undergo a valence tautomeric transition.[89] Small differences between HS Co-py and Co-tpp are expected due to distinct density of states (Fig. 1) and SCO transition temperatures. With a valence tautomerism-SCO transition temperature of 370 K, Co-tpp will retain a significant amount (<90%) of the LS Co-tpp in contrast to fully HS Co-py.[72] This estimate is based on magnetic susceptibility measurements and likely exceeds by a significant amount the actual value owing to X-ray induced electron excitations into the HS state.[72] The high-energy shoulder observed for all Co-py films is the result of three compared with four (Co-tpp) resonances discussed below (Fig. 4 and 5) that probably originate from the mixture of LS and HS states.[21,54,71] Both the XAS and XPS data suggest that the Co metal center in both tautomeric

systems is unaffected regardless of the molecular matrix and environment.

### 3.3 LUMO levels of Co-py

The unoccupied molecular orbitals of Co-py were experimentally identified by fitting the IPES and XAS spectra near the Co $L_3$ ($2p_{3/2}$) absorption edge with the smallest number of symmetric Gaussians. By these means, both resonance energy and relative weight of the electronic transitions are determined for correlation with theory and underlying substrate layer (Fig. 4, Table 2). The individual resonances, which are broadened by finite temperature effects and limited energy resolution, are labeled and color-coded as defined in Fig. 1a. IPES reveals all theoretically predicted ligand orbital levels, including those at 0 eV and with negligible metal weight (Fig. 4a) that are absent in XAS (Fig. 4b). Group IV corresponds to 4-CN-py and Co molecular orbitals with major contributions from the former (latter) appearing in IPES (XAS). The molecular orbitals of group IV are, according to DFT (Fig. 1a), not hybridized preventing an optically active LMCT state (Fig. 4c). Group V consists of unoccupied molecular orbitals of SQ, 4-CN-py, and Co that are both hybridized (Fig. 1a) and optically active (Fig. 4c). Both IPES and optical absorption spectroscopy hint at a continuous spectrum, *i.e.*, high density of orbital levels, at energies exceeding the numerically explored range (>5 eV). Comparing the final state configuration unveils excellent agreement between $E_3$ (XPS) and $E_{IV}$ (IPES) resonances, including, in particular, the substrate-dependent shift in binding energy of ≈0.5 eV for PANI and PDL with respect to HOPG (Tables 1 and 2).

### 3.4 LUMO levels of Co-tpp

Spectroscopy studies reveal five major differences between Co-tpp and Co-py: an enhanced resonance II; the existence of resonances III and E; an optically active LMCT state IV; and both cationic (PANI) and anionic (PDL) character corroborating the aforementioned XPS data. By analogy with Co-py, we observe resonances I and II in IPES mostly originating from SQ ligands (Fig. 5a). For Co-tpp, group II contains only SQ, while Co-py contains SQ and 4-CN-py orbital levels (Fig. 1b). To this extent, resonance II is significantly more prominent than theoretically predicted and even more pronounced when in contact with PANI. Samples on a PDL substrate layer reveal a reduced resonance II. The sizable modification of resonances associated with these low-lying LUMO levels divulges the expected dependence on the local environment, which is not taking into account by our *ab initio* calculations done for single Co-tpp molecule in vacuum. The third resonance in IPES at 2.5 to 3.5 eV (Fig. 5a, Table 2) corresponds to group III, *i.e.*, isolated 3-tpp ligand orbitals, that is absent in Co-py films. The corresponding 4-CN-py orbital levels in Co-py merge into group II (Fig. 1a). For PANI substrate layers, resonance III is shifted by 1 eV with respect to HOPG and PDL following a similar trend as the Co-weighted $E_3$ (XPS) and $E_{IV}$ (IPES) resonances. Both $E_3$ and $E_{IV}$ are roughly ±0.5 eV off for PANI and PDL with respect to HOPG (Tables 1 and 2) inferring a substrate-dependent cat-
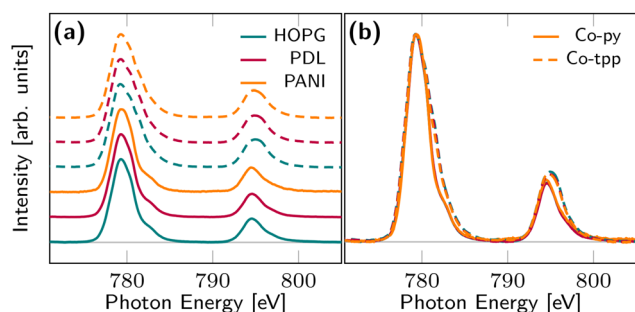


**Fig. 3** X-ray absorption spectra of HS Co-py and Co-tpp near the cobalt $2p_{3/2}$ absorption edges and at 300 K. (a) Spectra vertically shifted for visibility. Dashed (solid) curves refer to Co-tpp (Co-py) films. (b) Spectra overlayed revealing virtually the same electronic transitions for each tautomeric film independent of the substrate layer.
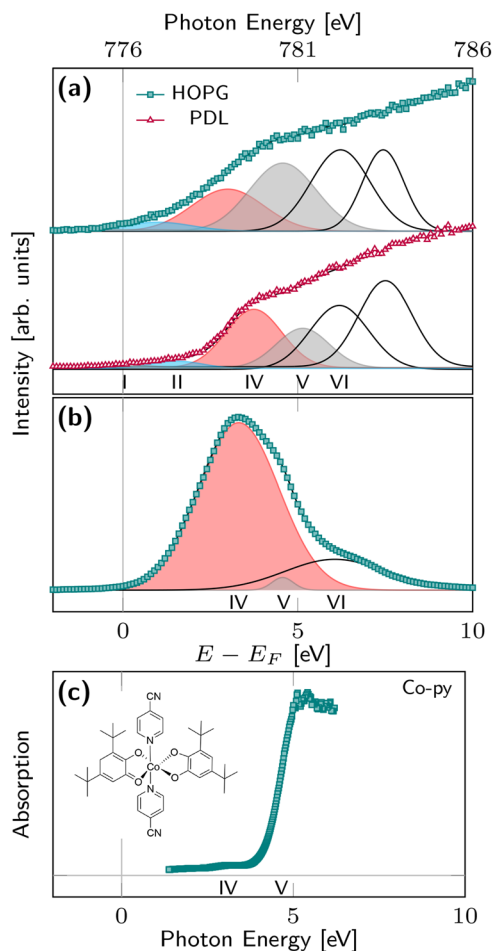
**Fig. 4** Absorption spectra of the unoccupied states of HS Co-py films recorded at 300 K using (a) inverse photoemission, (b) X-ray absorption, and (c) optical absorption spectroscopies. Spectra are plotted on both photon energy and relative energy scales to ensure compatibility with *ab initio* calculations. Relative energies are taken with respect to the binding energy (Fermi energy). Resonances are fitted with symmetric Gaussians and labeled using roman numerals according to Fig. 1. The total fitting curve is plotted behind the experimental data.



**Fig. 5** Absorption spectra of the unoccupied states of Co-tpp films recorded using (a) inverse photoemission, (b) X-ray absorption, and (c) optical absorption spectroscopies. X-ray absorption and inverse photoemission were recorded at 300 K; the optical absorption spectrum of HS Co-tpp on HOPG is taken at 400 K. Spectra are plotted on both photon energy and relative energy scales to ensure compatibility with *ab initio* calculations. Relative energies are taken with respect to the binding energy (Fermi energy). Resonances are fitted with symmetric Gaussians and labeled using roman numerals according to Fig. 1. Resonance E exclusively appearing in the X-ray and optical absorption indicates a secondary Co oxidation state, which is absent in Co-py films. The total fitting curve is plotted behind the experimental data.

ionic and anionic character without doping for PANI and PDL, respectively. Resonances IV, V, and VI appear in IPES and XAS (Fig. 5a and b) due to both ligand and cobalt weighted orbitals (Fig. 1b). In contrast to Co-py, the Co-tpp resonance IV is optically active due to orbital hybridization (Fig. 1b) representing the LMCT state at 4 eV (Fig. 5c). The optical absorption V at a photon energy of 4.5 eV also appears in IPES (Fig. 5a) and XAS (Fig. 5b) that corresponds, according to DFT (Fig. 1b), to a set of SQ and 3-tpp ligand levels with minor cobalt weight. Groups IV, V, and VI contribute in the same way (energy, weight, shape) to the XAS peak as in Co-py (Fig. 4b and 5b, Table 2). These resonances and orbitals are virtually unaffected by the local environment, *i.e.*, substrate layer, yielding the same XAS spectra (Fig. 2b). Resonance E exclusively appears in the X-ray and optical absorption of Co-tpp indicating a secondary Co oxidation state ≈2 eV off the main Co resonance IV. The
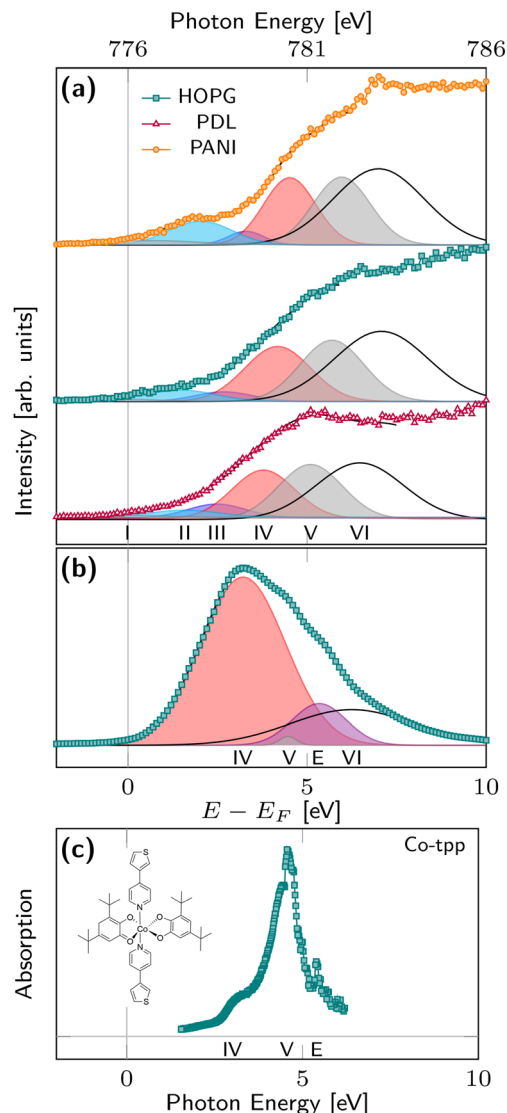
absence of a corresponding IPES resonance and weak optical absorption infer a negligible hybridization with ligand levels. This resonance likely represents the Co LS state with a smaller binding energy compared with the Co HS state.[21,54,71] As articulated above, the ratio of HS-to-LS state population (1/9) derived from magnetic susceptibility measurements (ESI Fig. 1†) is expected to underestimate the actual value in valence tautomerism-SCO molecules by a significant amount

**Table 2** Resonance energies and weights (integrals) for Co-py and Co-tpp films on different organic substrate layers retrieved from inverse photo-emission and X-ray absorption spectroscopies, depicted in Fig. 4 and 5. Energies are given relative to the Fermi level. Weights are in arbitrary, relative units. Cobalt resonances $E_{IV}$ in IPES show the same shift as $E_3$ in XPS. XAS values are the same for each substrate

| Substrate | $E_I$ [eV] | $I_I$ | $E_{II}$ [eV] | $I_{II}$ | $E_{III}$ [eV] | $I_{III}$ | $E_{IV}$ [eV] | $I_{IV}$ | $E_V$ [eV] | $I_V$ | $E_{VI}$ [eV] | $I_{VI}$ |
|---|---|---|---|---|---|---|---|---|---|---|---|---|
| **Co-py IPES** | | | | | | | | | | | | |
| HOPG | −0.1 | 0.1 | 1.0 | 0.16 | | | 3.0 | 0.80 | 4.6 | 1.20 | 6.2 | 1.27 |
| PDL | 0.0 | 0.0 | 1.6 | 0.17 | | | 3.8 | 0.89 | 5.1 | 0.59 | 6.2 | 1.06 |
| **Co-py XAS** | | | | | | | | | | | | |
| HOPG | | | | | | | 3.3 | 2.80 | 4.6 | 0.06 | 6.1 | 0.64 |
| **Co-tpp IPES** | | | | | | | | | | | | |
| HOPG | 0.0 | 0.04 | 1.5 | 0.20 | 2.7 | 0.14 | 4.2 | 0.93 | 5.8 | 1.01 | 7.0 | 1.68 |
| PDL | 0.0 | 0.04 | 1.6 | 0.13 | 2.5 | 0.22 | 3.8 | 0.80 | 5.1 | 0.94 | 6.5 | 1.27 |
| PANI | 0.5 | 0.12 | 2.1 | 0.39 | 3.4 | 0.13 | 4.5 | 0.90 | 5.9 | 1.00 | 7.0 | 1.77 |
| **Co-tpp XAS** | | | | | | | | | | | | |
| HOPG | | | | | $5.3^a$ | $0.44^a$ | 3.2 | 2.82 | 4.5 | 0.03 | 6.3 | 0.85 |

[a] Values are given for resonance $E$ exclusively appearing in the X-ray and optical absorption of Co-tpp samples associated with a secondary Co oxidation state ≈2 eV off the main resonance IV.

due to X-ray induced LS-to-HS state excitations[72] yielding a ratio of 6.4 (Table 2).

The existence of the LMCT states, unoccupied in the ground state, is essential for the optically driven transition from HS to LS state[90,91] since a direct excitation is forbidden by spin selection rules: $\Delta l = \pm 1$ (orbital moment) and $\Delta s = 0$ (spin moment). Given that the LMCT state for HS Co-tpp is 4 eV above the chemical potential (Fig. 1 and 5, Table 2) with a corresponding LS state seen in theory, excitations from the ground state should be in the near ultraviolet, *i.e.*, <410 nm. This estimate ignores the Coulomb interaction between the photohole and the excited-state electron, which can lead to optical absorption at much lower energies. The optical absorption suggests, though, that these effects are modest (Fig. 5c). While the HOMO to LUMO gap might not be large, as evident from the unoccupied density of states just above the chemical potential (Fig. 5a), transitions to the LMCT state require larger excitation energies and may explain why X-rays are so effectively converting LS Co-tpp to HS Co-tpp. Relevant to prospective optoelectronics applications, the LMCT states are virtually unaffected when Co-tpp is placed adjacent to a PANI or PDL molecular layer despite profoundly enhancing conductivity and mobility.[29]

## 4 Conclusions

The electronic structures and spin states of HS Co-py and Co-tpp films remain, according to IPES, XPS, and XAS to a great extent, unperturbed by either an adjacent PANI or PDL thin film. Alteration of the electronic structure are limited to slight modifications to binding energy, *i.e.*, cationic and anionic character, and shifted orbital levels. No sizable change in the Co 2p absorption spectra is observed corroborating an electronic structure of the central Co atom that is unaffected by the environment. Comparing density functional theory with IPES, XAS, and optical absorption spectra after spectroscopic core level alignment, reveals a remarkable agreement and indicates the existence of an optically active ligand-to-metal charge transfer (LMCT) state in Co-tpp that are absent near the Fermi level in HS Co-py. The spin-polarized, delocalized LMCT state originates from the hybridization of 3-tpp and Co orbitals and bears great potential for magnetoresistive applications. This is the first experimental evidence of the commonly invoked LMCT or metal-to-ligand charge transfer (MLCT) states in SCO and valence tautomerism-SCO molecules.

## Author contributions

Conceptualization, E. M., T. K. E. and P. A. D.; methodology, E. M., T. S. R., R. S., and P. A. D.; software, E. M., T. K. E., T. P., D. L., T. S. R., A. T. N. and R. S.; validation, E. M., T. K. E., T. P., D. L., T. S. R., R. S. and P. A. D.; formal analysis, E. M., T. P., D. L., T. S. R., R. S. and P. A. D.; investigation, E. M., T. K. E., T. P., D. L., T. S. R., J. P. P., M. Z. Z., S. Y., P. W., K. A. M. and A. T. N., resources, A. T. N., R. Y. L., R. C., M. S. and P. A. D.; data curation, E. M., D. L., T. S. R. and P. A. D.; writing – original draft, E. M., R. S., D. L. and P. A. D.; writing – review and editing, E. M., M. S., R. S. and P. A. D.; visualization, R. S. and P. A. D.; supervision, R. Y. L., M. S., R. S., R. C. and P. A. D.; project administration, P. A. D., T. S. R. and R. S.; funding acquisition, T. S. R., R. S., R. Y. L., R. C., and P. A. D. All authors have read and agreed to the published version of the manuscript.

## Conflicts of interest

There are no conflicts to declare.

## Acknowledgements

# References

1 P. Gütlich, Y. Garcia and H. A. Goodwin, *Chem. Soc. Rev.*, 2000, **29**, 419–427.

2 E. Evangelio and D. Ruiz-Molina, *C. R. Chim.*, 2008, **11**, 1137–1154.

3 O. Sato, J. Tao and Y. Zhang, *Angew. Chem., Int. Ed.*, 2007, **46**, 2152–2187.

4 T. Tezgerevska, K. G. Alley and C. Boskovic, *Coord. Chem. Rev.*, 2014, **268**, 23–40.

5 O. Drath, R. W. Gable, B. Moubaraki, K. S. Murray, G. Poneti, L. Sorace and C. Boskovic, *Inorg. Chem.*, 2016, **55**, 4141–4151.

6 D. M. Adams, A. Dei, A. L. Rheingold and D. N. Hendrickson, *J. Am. Chem. Soc.*, 1993, **115**, 8221–8229.

7 D. M. Adams, A. Dei, A. L. Rheingold and D. N. Hendrickson, *Angew. Chem., Int. Ed.*, 1993, **32**, 880–882.

8 P. Gütlich and A. Dei, *Angew. Chem., Int. Ed.*, 1997, **36**, 2734–2736.

9 O. Sato, S. Hayami, Z. Z. Gu, K. Takahashi, R. Nakajima and A. Fujishima, *Chem. Phys. Lett.*, 2002, **355**, 169–174.

10 H. W. Liu, K. Matsuda, Z. Z. Gu, K. Takahashi, A. L. Cui, R. Nakajima, A. Fujishima and O. Sato, *Phys. Rev. Lett.*, 2003, **90**, 167403.

11 O. Cador, F. Chabre, A. Dei, C. Sangregorio, J. V. Slageren and M. G. F. Vaz, *Inorg. Chem.*, 2003, **42**, 6432–6440.

12 C. Carbonera, A. Dei, J.-F. Létard, C. Sangregorio and L. Sorace, *Angew. Chem.*, 2004, **116**, 3198–3200.

13 D. N. Hendrickson and C. G. Pierpont, *Spin Crossover in Transition Metal Compounds II*, 2004, 63–95.

14 O. Sato, A. Cui, R. Matsuda, J. Tao and S. Hayami, *Acc. Chem. Res.*, 2007, **40**, 361–369.

15 A. Dei and L. Sorace, *Appl. Magn. Reson.*, 2010, **38**, 139–153.

16 Y. Mulyana, G. Poneti, B. Moubaraki, K. S. Murray, B. F. Abrahams, L. Sorace and C. Boskovic, *Dalton Trans.*, 2010, **39**, 4757–4767.

17 R. D. Schmidt, D. A. Shultz and J. D. Martin, *Inorg. Chem.*, 2010, **49**, 3162–3168.

18 K. G. Alley, G. Poneti, J. B. Aitken, R. K. Hocking, B. Moubaraki, K. S. Murray, B. F. Abrahams, H. H. Harris, L. Sorace and C. Boskovic, *Inorg. Chem.*, 2012, **51**, 3944–3946.

19 A. Calzolari, Y. Chen, G. F. Lewis, D. B. Dougherty, D. Shultz and M. Buongiorno Nardelli, *J. Phys. Chem. B*, 2012, **116**, 13141–13148.

20 K. G. Alley, G. Poneti, P. S. D. Robinson, A. Nafady, B. Moubaraki, J. B. Aitken, S. C. Drew, C. Ritchie, B. F. Abrahams, R. K. Hocking, K. S. Murray, A. M. Bond, H. H. Harris, L. Sorace and C. Boskovic, *J. Am. Chem. Soc.*, 2013, **135**, 8304–8323.

21 G. Poneti, M. Mannini, B. Cortigiani, L. Poggini, L. Sorace, E. Otero, P. Sainctavit, R. Sessoli and A. Dei, *Inorg. Chem.*, 2013, **52**, 11798–11805.

22 O. Drath and C. Boskovic, *Coord. Chem. Rev.*, 2018, **375**, 256–266.

23 G. K. Gransbury, B. N. Livesay, J. T. Janetzki, M. A. Hay, R. W. Gable, M. P. Shores, A. Starikova and C. Boskovic, *J. Am. Chem. Soc.*, 2020, **142**, 10692–10704.

24 G. Hao, A. Mosey, X. Jiang, A. J. Yost, K. R. Sapkota, G. T. Wang, X. Zhang, J. Zhang, A. T. N'Diaye, R. Cheng, X. Xu and P. A. Dowben, *Appl. Phys. Lett.*, 2019, **114**, 032901.

25 A. Mosey, A. S. Dale, G. Hao, A. N'Diaye, P. A. Dowben and R. Cheng, *J. Phys. Chem. Lett.*, 2020, **11**, 8231–8237.

26 T. K. Ekanayaka, G. Hao, A. Mosey, A. S. Dale, X. Jiang, A. J. Yost, K. R. Sapkota, G. T. Wang, J. Zhang, A. T. N'Diaye, A. Marshall, R. Cheng, A. Naeemi, X. Xu and P. A. Dowben, *Magnetochemistry*, 2021, **7**, 37.

27 C. Lefter, I. A. Gural'skiy, H. Peng, G. Molnár, L. Salmon, A. Rotaru, A. Bousseksou and P. Demont, *Phys. Status Solidi RRL*, 2014, **8**, 191–193.

28 D. Nieto-Castro, F. A. Garcés-Pineda, A. Moneo-Corcuera, I. Sánchez-Molina and J. R. Galán-Mascarós, *Adv. Funct. Mater.*, 2021, **31**, 2102469.

29 E. Mishra, T. K. Ekanayaka, K. A. McElveen, R. Y. Lai and P. A. Dowben, *Org. Electron.*, 2022, **105**, 106516.

30 H. Phan, S. M. Benjamin, E. Steven, J. S. Brooks and M. Shatruk, *Int. Ed.*, 2015, **54**, 823–827.

31 Y. N. Shvachko, D. V. Starichenko, A. V. Korolyov, E. B. Yagubskii, A. I. Kotov, L. I. Buravov, K. A. Lyssenko, V. N. Zverev, S. V. Simonov, L. V. Zorina, O. G. Shakirova and L. G. Lavrenova, *Inorg. Chem.*, 2016, **55**, 9121–9130.

32 Y. N. Shvachko, D. V. Starichenko, A. V. Korolyov, A. I. Kotov, L. I. Buravov, V. N. Zverev, S. V. Simonov, L. V. Zorina and E. B. Yagubskii, *Magnetochemistry*, 2017, **3**, 9.

33 A. V. Kazakova, A. V. Tiunova, D. V. Korchagin, G. V. Shilov, E. B. Yagubskii, V. N. Zverev, S. C. Yang, J.-Y. Lin, J.-F. Lee, O. V. Maximova and A. N. Vasiliev, *Chem. – Eur. J.*, 2019, **25**, 10204–10213.

34 V. Rubio-Giménez, S. Tatay and C. Martí-Gastaldo, *Chem. Soc. Rev.*, 2020, **49**, 5601–5638.

35 R. Ishikawa, S. Ueno, S. Nifuku, Y. Horii, H. Iguchi, Y. Miyazaki, M. Nakano, S. Hayami, S. Kumagai, K. Katoh, Z.-Y. Li, M. Yamashita and S. Kawata, *Chem. – Eur. J.*, 2020, **26**, 1278–1285.

36 Ö. Üngör, E. S. Choi and M. Shatruk, *Chem. Sci.*, 2021, **12**, 10765–10779.

37 M. Wang, Z.-Y. Li, R. Ishikawa and M. Yamashita, *Coord. Chem. Rev.*, 2021, **435**, 213819.

38 S. Hayami, Y. Komatsu, T. Shimizu, H. Kamihata and Y. H. Lee, *Coord. Chem. Rev.*, 2011, **255**, 1981–1990.

39 M. Maskus and H. D. Abruña, *Langmuir*, 1996, **12**, 4455–4462.

40 J. Park, A. N. Pasupathy, J. I. Goldsmith, C. Chang, Y. Yaish, J. R. Petta, M. Rinkoski, J. P. Sethna, H. D. Abruña, P. L. McEuen and D. C. Ralph, *Nature*, 2002, **417**, 722–725.

41 M. G. Cowan, J. Olguín, S. Narayanaswamy, J. L. Tallon and S. Brooker, *J. Am. Chem. Soc.*, 2012, **134**, 2892–2894.

42 M. G. Cowan, R. G. Miller and S. Brooker, *Dalton Trans.*, 2015, **44**, 2880–2892.

43 M. S. Bennington, H. L. C. Feltham, Z. J. Buxton, N. G. White and S. Brooker, *Dalton Trans.*, 2017, **46**, 4696–4710.

44 F. N. H. Karabulut, H. L. C. Feltham and S. Brooker, *Dalton Trans.*, 2018, **47**, 11749–11759.

45 J. N. McPherson, R. W. Hogue, F. S. Akogun, L. Bondì, E. T. Luis, J. R. Price, A. L. Garden, S. Brooker and S. B. Colbran, *Inorg. Chem.*, 2019, **58**, 2218–2228.

46 A. Droghetti and S. Sanvito, *Phys. Rev. Lett.*, 2011, **107**, 047201.

47 R. M. Buchanan and C. G. Pierpont, *J. Am. Chem. Soc.*, 1980, **102**, 4951–4957.

48 O.-S. Jung and C. G. Pierpont, *J. Am. Chem. Soc.*, 1994, **116**, 1127–1128.

49 O.-S. Jung and C. G. Pierpont, *J. Am. Chem. Soc.*, 1994, **116**, 2229–2230.

50 C. G. Pierpont and O.-S. Jung, *Inorg. Chem.*, 1995, **34**, 4281–4283.

51 D. M. Adams and D. N. Hendrickson, *J. Am. Chem. Soc.*, 1996, **118**, 11515–11528.

52 D. M. Adams, L. Noodleman and D. Hendrickson, *Inorg. Chem.*, 1997, **36**, 3966–3984.

53 F. Varret, M. Nogues and A. Goujon, *Photomagnetic Properties of Some Inorganic Solids*, John Wiley & Sons, Ltd, 2001, ch. 8, pp. 257–295.

54 T. Yokoyama, K. Okamoto, K. Nagai, T. Ohta, S. Hayami, Z.-Z. Gu, R. Nakajima and O. Sato, *Chem. Phys. Lett.*, 2001, **345**, 272–276.

55 O. Sato, S. Hayami, Z.-Z. Gu, K. Seki, R. Nakajima and A. Fujishima, *Chem. Lett.*, 2001, **30**, 874–875.

56 O. Sato, S. Hayami, Z. Z. Gu, K. Takahashi, R. Nakajima and A. Fujishima, *Phase Transitions*, 2002, **75**, 779–785.

57 O. Sato, S. Hayami, Z.-Z. Gu, K. Takahashi, R. Nakajima, K. Seki and A. Fujishima, *J. Photochem. Photobiol., A*, 2002, **149**, 111–114.

58 A. Cui, K. Takahashi, A. Fujishima and O. Sato, *J. Photochem. Photobiol., A*, 2004, **161**, 243–246.

59 A. Cui, K. Takahashi, A. Fujishima and O. Sato, *J. Photochem. Photobiol., A*, 2004, **167**, 69–73.

60 S. Bin-Salamon, S. Brewer, S. Franzen, D. L. Feldheim, S. Lappi and D. A. Shultz, *J. Am. Chem. Soc.*, 2005, **127**, 5328–5329.

61 J. Tao, H. Maruyama and O. Sato, *J. Am. Chem. Soc.*, 2006, **128**, 1790–1791.

62 A. Beni, A. Dei, D. Shultz and L. Sorace, *Chem. Phys. Lett.*, 2006, **428**, 400–404.

63 A. Beni, A. Dei, M. Rizzitano and L. Sorace, *Chem. Commun.*, 2007, 2160–2162.

64 P. Dapporto, A. Dei, G. Poneti and L. Sorace, *Chem. – Eur. J.*, 2008, **14**, 10915–10918.

65 R. D. Schmidt, D. A. Shultz, J. D. Martin and P. D. Boyle, *J. Am. Chem. Soc.*, 2010, **132**, 6261–6273.

66 B. Li, L.-Q. Chen, R.-J. Wei, J. Tao, R.-B. Huang, L.-S. Zheng and Z. Zheng, *Inorg. Chem.*, 2011, **50**, 424–426.

67 X.-Y. Chen, R.-J. Wei, L.-S. Zheng and J. Tao, *Inorg. Chem.*, 2014, **53**, 13212–13219.

68 M. Slota, M. Blankenhorn, E. Heintze, M. Vu, R. Hübner and L. Bogani, *Faraday Discuss.*, 2015, **185**, 347–359.

69 T. M. Francisco, W. J. Gee, H. J. Shepherd, M. R. Warren, D. A. Shultz, P. R. Raithby and C. B. Pinheiro, *J. Phys. Chem. Lett.*, 2017, **8**, 4774–4778.

70 H. W. Liang, T. Kroll, D. Nordlund, T.-C. Weng, D. Sokaras, C. G. Pierpont and K. J. Gaffney, *Inorg. Chem.*, 2017, **56**, 737–747.

71 A. Guda, M. Chegerev, A. Starikov, V. Vlasenko, A. Zolotukhin, M. Bubnov, V. Cherkasov, V. Shapovalov, Y. V. Rusalev, A. Tereshchenko, A. Trigub, A. Chernyshev and A. Soldatov, *J. Phys.: Condens. Matter*, 2021, **33**, 215405.

72 T. K. Ekanayaka, P. Wang, S. Yazdani, J. P. Phillips, E. Mishra, A. S. Dale, A. T. N'Diaye, C. Klewe, P. Shafer, J. Freeland, R. Streubel, J. P. Wampler, V. Zapf, R. Cheng, M. Shatruk and P. A. Dowben, *Chem. Commun.*, 2022, **58**, 661.

73 L. Kipgen, M. Bernien, F. Nickel, H. Naggert, A. J. Britton, L. M. Arruda, E. Schierle, E. Weschke, F. Tuczek and W. Kuch, *J. Phys.: Condens. Matter*, 2017, **29**, 394003.

74 R. Ansell, T. Dickinson, A. Povey and P. Sherwood, *J. Electroanal. Chem.*, 1979, **98**, 79–89.

75 R. Streubel, A. T. N'Diaye, K. Srinivasan, A. Kalitsov, S. Jain, A. Ajan and P. Fischer, *J. Phys.: Condens. Matter*, 2021, **33**, 104003.

76 P. E. Blöchl, *Phys. Rev. B: Condens. Matter Mater. Phys.*, 1994, **50**, 17953–17979.

77 G. Kresse and D. Joubert, *Phys. Rev. B: Condens. Matter Mater. Phys.*, 1999, **59**, 1758–1775.

78 G. Kresse and J. Furthmüller, *Comput. Mater. Sci.*, 1996, **6**, 15.

79 J. Heyd, G. E. Scuseria and M. Ernzerhof, *J. Chem. Phys.*, 2003, **118**, 8207–8215.

80  J. Heyd, G. E. Scuseria and M. Ernzerhof, *J. Chem. Phys.*, 2006, **124**, 219906.

81  P. Borlido, J. Schmidt, A. W. Huran, F. Tran, M. A. L. Marques and S. Botti, *npj Comput. Mater.*, 2020, **6**, 96.

82  C. Dugan, L. Wang, K. Zhang, J. M. Mann, M. M. Kimani, W.-N. Mei, P. A. Dowben and J. Petrosky, *Phys. Status Solidi B*, 2022, **259**, 2200238.

83  J. P. Perdew, K. Burke and M. Ernzerhof, *Phys. Rev. Lett.*, 1996, **77**, 3865.

84  J. P. Perdew, K. Burke and M. Ernzerhof, *Phys. Rev. Lett.*, 1997, **78**, 1396.

85  S. Grimme, J. Antony, S. Ehrlich and H. Krieg, *J. Chem. Phys.*, 2010, **132**, 154104.

86  S. L. Dudarev, G. A. Botton, S. Y. Savrasov, C. J. Humphreys and A. P. Sutton, *Phys. Rev. B: Condens. Matter Mater. Phys.*, 1998, **57**, 1505–1509.

87  C. Borca, T. Komesu and P. Dowben, *J. Electron Spectrosc. Relat. Phenom.*, 2002, **122**, 259–273.

88  T. K. Ekanayaka, H. Kurz, K. A. McElveen, G. Hao, E. Mishra, A. T. N'Diaye, R. Y. Lai, B. Weber and P. A. Dowben, *Phys. Chem. Chem. Phys.*, 2022, **24**, 883–894.

89  N. Bouldi, M. Mannini, M. Retegan, R. G. Miller, B. Cahier, P. Sainctavit, N. Guihéry, T. Mallah, D. Cabaret, D. Gouéré, F. Baudelet, L. Nataf, F. Wilhelm, F. Guillou, A. Rogalev, N. Suaud, S. Brooker and A. Juhin, *J. Phys. Chem. C*, 2022, **126**, 5784–5792.

90  N. Huse, H. Cho, T. K. Kim, L. Jamula, J. K. McCusker, F. de Groot and R. W. Schoenlein, International Conference on Ultrafast Phenomena, 2010, p. TuD2.

91  W. Zhang, K. S. Kjær, R. Alonso-Mori, U. Bergmann, M. Chollet, L. A. Fredin, R. G. Hadt, R. W. Hartsock, T. Harlang, T. Kroll, K. Kubiček, H. T. Lemke, H. W. Liang, Y. Liu, M. M. Nielsen, P. Persson, J. S. Robinson, E. I. Solomon, Z. Sun, D. Sokaras, T. B. van Driel, T.-C. Weng, D. Zhu, K. Wärnmark, V. Sundström and K. J. Gaffney, *Chem. Sci.*, 2017, **8**, 515–523.